Circular Ports in Parallel-Plate Waveguide Analysis With Isotropic Excitations

Xiaomin Duan, *Student Member, IEEE*, Renato Rimolo-Donadio, *Member, IEEE*, Heinz-Dietrich Brüns, and Christian Schuster, *Senior Member, IEEE*

***Abstract*—Exact and consistent modeling of circularly shaped ports in the power/ground plane analysis under the assumption of isotropic excitations is addressed in this paper. Novel expressions are first derived for accurate calculation of the parallel-plate impedance of circular ports in the cavity resonator method. These ports are usually approximated as either rectangular or linear ones, leading to inaccurate results at high frequencies. The second part of this paper develops a novel semianalytical approach, derived from the contour integral equation, for modeling of circular ports assuming infinitely large reference planes. It will be shown that the radial waveguide method is a low frequency approximation of our approach and neglects the scattering among the open ports. The analytical solutions for infinite planes are then combined with the contour integral method to model finite-sized power planes. This improves the computational efficiency since a discretization of circular ports is avoided, especially for problems with a large number of circular ports.**

***Index Terms*—Cavity resonator (CR) method, contour integral method (CIM), cylindrical wave function, parallel-plate waveguide, power integrity, printed circuit board (PCB), signal integrity.**

I. Introduction

PARALLEL-PLATE waveguide structures are commonly found in high-speed electronic systems, formed, for instance, by the power/ground planes of printed circuit boards (PCBs). The switching noise, caused by currents drawn at the ports, where ICs and other components are connected to the power supply, can lead to signal integrity, power integrity, and electromagnetic interference problems [1]–[3]. Therefore, accurate determination of the impedances at the ports becomes critical for the power delivery network design and modeling.

A number of techniques have been proposed and applied for rapid calculation of the parallel-plate impedance Z_{pp} of power/ground plane structures [4]–[21]. In previous works, extensive effort has been devoted to the modeling of the power planes. However, as the operating frequency of digital systems increases and rise/fall time drops, the bandwidth has been broadened to even higher frequencies. For example, 25 Gb/s on-board signaling is considered in [22]. The third harmonic of a 25 Gb/s bit rate corresponds to 37.5 GHz. At such frequencies, the size of the port may be a considerable fraction of the wavelength. Hence, accurate modeling of Z_{pp} becomes more and more an issue, especially for signal integrity analysis, since many efficient via and system-level models use Z_{pp} as a building block and their validity depends on the accuracy of Z_{pp} calculation [23]–[27]. This paper focuses on developing analytical expressions for accurate Z_{pp} calculation of circular ports in the cavity resonator (CR) model as well as in the contour integral method (CIM) under the assumption of isotropic excitations on ports.

The CR method is a popular approach for the power bus modeling, where the power/ground plane pairs are considered as CRs and their impedances are expressed by summations over the cavity modes [4]–[10]. Circular ports are usually approximated as rectangular or linear shapes of equivalent sizes. However, this approximation is only accurate up to the frequency where the wavelength is much larger than the port size. Therefore, a new expression for true circular ports in the CR model is derived to improve the accuracy. In comparison to the old formulation, where ports are related to *sinc* functions, the new formula contains Bessel functions. Furthermore, the solution domain of Z_{pp} is a plane pair with perfect magnetic conductor (PMC) holes, whose Green's function is in general not known. We use Green's function for solid planes and include the effect of the PMC holes by the desegmentation technique [28].

Another fast method, CIM, is a numerical technique that was developed for handling of arbitrary-shaped power planes [4], [18]–[20]. One way to model circular ports in CIM is to discretize the port perimeter into a finite number of segments, whose widths are much smaller than the wavelength [18]. However, for higher frequencies, the computation effort can increase significantly since more segments are needed for accurate modeling of each port. Therefore, we develop a semianalytical approach, where the ports are associated with analytical representations, to alleviate the computation burden by avoiding fine discretization of the ports. We start with the derivation for infinite planes and show that the radial waveguide (RW) method [10]–[13] is a low frequency approximation of our approach. We then combine these solutions with the conventional CIM to include finite planes.

In summary, the main contributions of this paper are novel expressions for accurate impedance calculation of circular ports in the CR model, analytical solutions for circular ports in the CIM that improve the computation efficiency in comparison to

Manuscript received June 24, 2010; revised May 4, 2011; accepted September 14, 2011. Date of publication November 15, 2011; date of current version June 15, 2012.

The authors are with the Institut für Theoretische Elektrotechnik, Technische Universität Hamburg-Harburg, 21073 Hamburg, Germany (e-mail: xiaomin.duan@tu-harburg.de; renato.rimolo@tuhh.de; bruens@tu-harburg.de; schuster@tu-harburg.de).

Color versions of one or more of the figures in this paper are available online at http://ieeexplore.ieee.org.

Digital Object Identifier 10.1109/TEMC.2011.2170998

0018-9375/$26.00 © 2011 IEEE
Authorized licensed use limited to: Missouri University of Science and Technology. Downloaded on October 21,2024 at 21:00:28 UTC from IEEE Xplore. Restrictions apply.

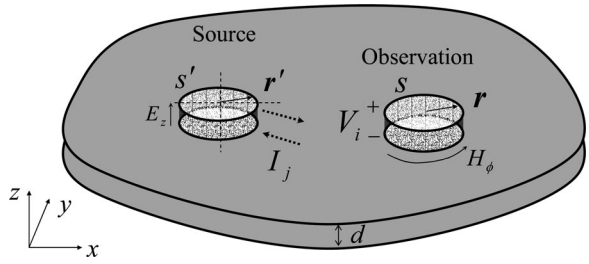

Fig. 1. Illustration of the circular port definition.

the conventional CIM, and accounting for the effect of scattered fields among ports by both of the methods in contrast to the RW method.

II. Circular Port Definition

In the following, we adopt the definitions and assumptions of the circularly shaped ports in [21]. For clarity, it is repeated here briefly. Fig. 1 illustrates a two-port power bus with its height denoted as d. $\boldsymbol{r}$ and $\boldsymbol{r}'$ represent vectors on the observation and source ports i and j, respectively. It is assumed that d is small in comparison to the wavelength, so that fields can be considered constant in z-direction across the whole power bus. The circular port is specified as a cylindrical area facing toward the power bus, as shown in Fig. 1. In the following, we assume first that the excitation current and voltage at source port j are isotropic and constant over the rotationally symmetric circular port, i.e., the tangential electric and magnetic fields E_z and H_ϕ do not vary along the perimeter of the port. Hence, in the local cylindrical coordinate of the source port with its origin at the port center, we can define

$$V_j = -E_z(a_j)\cdot d, \quad I_j = -H_\phi(a_j)\cdot 2\pi a_j \tag{1}$$

where a_j is the radius of port j. The tangential electric and magnetic fields on the observation port i can be location dependent and the voltage and current are defined as a line average of the tangential electric and magnetic fields along the circumference of the port i [21]

$$V_i = -\frac{d}{2\pi a_i}\cdot\oint_s E_z(\boldsymbol{r})ds, \quad I_i = -\oint_s H_\phi(\boldsymbol{r})ds \tag{2}$$

where a_i is the radius of port i. From (1) and (2), it is easy to find the parallel-plate impedance Z_{pp}

$$Z_{ij} = \frac{V_i}{I_j} = \frac{d}{2\pi a_i}\cdot\frac{\oint_s E_z(\boldsymbol{r})ds}{2\pi a_j\cdot H_\phi(a_j)}. \tag{3}$$

Since the line integral in (3) averages out any higher order anisotropic field distribution, Z_{pp} is here defined with respect to the fundamental isotropic mode of the fields on the port. Under the assumptions in (1), (2), and (3), the impedance expression for infinite plane pairs can be derived using the zeroth-order cylindrical wave expansion function, as in the RW method [11]–[13]

$$Z_{ij} = \frac{j\eta d}{2\pi a_j\cdot H_1^{(2)}(ka_j)}\cdot\begin{cases} H_0^{(2)}(ka_j) & (i=j)\\ J_0(ka_i)H_0^{(2)}(kR) & (i\neq j)\end{cases} \tag{4}$$

where $H_0^{(2)}$ and $H_1^{(2)}$ are the zeroth-order and first-order Hankel function of the second kind, respectively. J_0 denotes the zeroth-order Bessel function. The distance between centers of the ports is represented by R. k is the complex wavenumber including dielectric and ohmic losses, as defined in [4]. η denotes the complex wave impedance. In comparison to the formulation in [11] and [12], an additional zeroth-order Bessel function is included for the transfer impedance in (4), resulting from the integral over the circumference of the observation port as in (3). This has also been reported in [13].

III. CR Model With Circular Ports

In the CR model, due to the specific geometry of the power-plane structure, the impedance can be calculated by integrating the Green's function and taking an average over a rectangular port area, as described in [5]. However, very often the physical geometry of the ports is circular, especially for applications involving vias. Under the isotropic excitation assumption, the tangential magnetic field on the area of source port j is considered constant and an equivalent sheet current in the z-direction can be defined as $J_z = H_\phi$. The electric field along the circumference of port i can then be described by the electric field integral equation

$$E_z(r) = \oint_{s'} H_\phi\cdot G(\boldsymbol{r},\boldsymbol{r}')ds \tag{5}$$

where $G(\boldsymbol{r}, \boldsymbol{r}')$ is the Green's function of the 2-D Helmholz equation [4]. For a rectangular cavity with PMC boundary

$$\begin{aligned} G(\boldsymbol{r},\boldsymbol{r}') &= G(x,y,x',y')\\ &= \frac{j\mu\omega}{P_xP_y}\cdot\sum_{m=0}^{\infty}\sum_{n=0}^{\infty}\frac{C_m^2C_n^2}{k_{xm}^2+k_{yn}^2-k^2}\\ &\quad\cdot\cos(k_{xm}x')\cos(k_{yn}y')\cos(k_{xm}x)\cos(k_{yn}y) \end{aligned} \tag{6}$$

where P_x and P_y are the plane widths in the x- and y-direction, respectively. μ denotes the permeability and ω is the angular frequency. m and n represent the mth and nth eigenmode in the x- and y-direction, respectively, whereas $C_{m,n} = 1$ if $m, n = 0$ and $C_{m,n} = \sqrt{2}$ if $m, n \neq 0$. $k_{xm} = m\pi/P_x$ and $k_{yn} = n\pi/P_y$. Substituting (5) into the impedance definition (3), Z_{pp} can then be expressed as

$$Z_{ij} = \frac{d}{2\pi\, a_i\cdot 2\pi\, a_j}\cdot\oint_{c_i} ds\cdot\oint_{c_j} ds'\cdot G(\boldsymbol{r},\boldsymbol{r}') \tag{7}$$

where c_j and c_i are the circumferences of the source and observation ports, respectively, as shown in Fig. 2. Equation (7) can

Authorized licensed use limited to: Missouri University of Science and Technology. Downloaded on October 21,2024 at 21:00:28 UTC from IEEE Xplore. Restrictions apply.

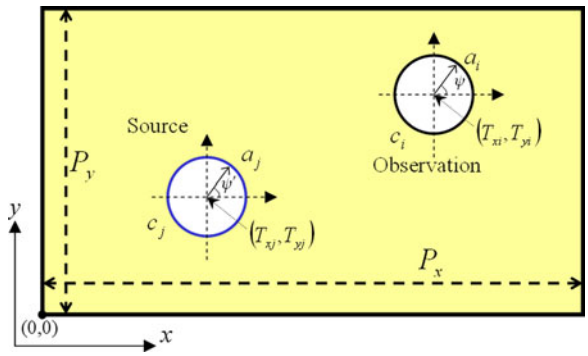

Fig. 2. Top view of a rectangular power-plane structure with two ports and parameter definition for circular ports in the cavity model.

be explicitly written as

$$Z_{ij} = \frac{j\mu\omega d}{P_x P_y} \cdot \sum_{n=0}^{\infty}\sum_{m=0}^{\infty} \frac{C_n^2 C_m^2}{k_{xm}^2 + k_{yn}^2 - k^2} \cdot \frac{1}{2\pi} \underbrace{\int_0^{2\pi} \cos(k_{yn}T_{yi} + a_i\cos\psi)\cdot\cos(k_{xm}T_{xi} + a_i\sin\psi)\cdot d\psi}_{\alpha_1} \cdot \frac{1}{2\pi} \underbrace{\int_0^{2\pi} \cos(k_{yn}T_{yj} + a_j\cos\psi')\cdot\cos(k_{xm}T_{xj} + a_j\cos\psi')\cdot d\psi'}_{\alpha_2} \tag{8}$$

where (T_{xj}, T_{yj}) and (T_{xi}, T_{yi}) are the coordinates of the centers of the source and observation ports, respectively. ψ and ψ' are the angles in the local coordinates of observation and source circles, as shown in Fig. 2. The two integrals in (8) are of the same form and can be solved similarly. Applying the addition formula for cosine functions, α_1 can be decomposed into

$$\alpha_1 = K_1 + K_2 + K_3 + K_4 \tag{9}$$

where

$$K_1 = \cos(k_{xm}T_{xi})\cos(k_{yn}T_{yi}) \times \int_0^{2\pi} \cos(k_{xm}a_i\cos\psi)\cos(k_{yn}a_i\sin\psi)\cdot d\psi$$

$$K_2 = \sin(k_{xm}T_{xi})\sin(k_{yn}T_{yi}) \times \int_0^{2\pi} \sin(k_{xm}a_i\cos\psi)\sin(k_{yn}a_i\sin\psi)\cdot d\psi$$

$$K_3 = \cos(k_{xm}T_{xi})\sin(k_{yn}T_{yi}) \times \int_0^{2\pi} \cos(k_{xm}a_i\cos\psi)\sin(k_{yn}a_i\sin\psi)\cdot d\psi$$

$$K_4 = \sin(k_{xm}T_{xi})\cos(k_{yn}T_{yi}) \times \int_0^{2\pi} \sin(k_{xm}a_i\cos\psi)\cos(k_{yn}a_i\sin\psi)\cdot d\psi.$$

The aforementioned integrals in K_1–K_4 can be solved with the assistance of the following generating functions [29]:

$$\cos(z\cdot\cos\theta) = \sum_{k=-\infty}^{\infty} (-1)^k \cdot J_{2k}(z)\cdot\cos(2k\theta) \tag{10}$$

$$\cos(z\cdot\sin\theta) = \sum_{k=-\infty}^{\infty} J_{2k}(z)\cdot\cos(2k\theta) \tag{11}$$

$$\sin(z\cdot\cos\theta) = 2\cdot\sum_{k=0}^{\infty} (-1)^k \cdot J_{2k+1}(z)\cdot\cos[(2k+1)\theta] \tag{12}$$

$$\sin(z\cdot\sin\theta) = 2\cdot\sum_{k=0}^{\infty} J_{2k+1}(z)\cdot\sin[(2k+1)\theta]. \tag{13}$$

Substituting (10) and (11) into the integral for K_1 yields

$$K_1 = \cos(k_{xm}T_{xi})\cos(k_{yn}T_{yi}) \cdot \sum_{p=-\infty}^{\infty}\sum_{q=-\infty}^{\infty} (-1)^p J_{2p}(k_{xm}a_i)J_{2q}(k_{yn}a_i) \times \int_0^{2\pi} \cos(2p\psi)\cos(2q\psi)d\psi. \tag{14}$$

The integral in (14) is only nonzero when $|p| = |q|$, leading to

$$K_1 = 2\pi\cdot\cos(k_{xm}T_{xi})\cos(k_{yn}T_{yi}) \cdot \left[J_0(k_{xm}a_i)\cdot J_0(k_{yn}a_i) + 2\cdot\sum_{p=1}^{\infty}(-1)^p J_{2p}(k_{xm}a_i)J_{2p}(k_{yn}a_i)\right]. \tag{15}$$

Applying the addition theorem for Bessel functions [30]

$$J_0(\sqrt{\alpha^2+\beta^2}) = J_0(\alpha)\cdot J_0(\beta) + 2\cdot\sum_{k=1}^{\infty}(-1)^k J_{2k}(\alpha)J_{2k}(\beta). \tag{16}$$

K_1 can be simplified as

$$K_1 = 2\pi\cdot\cos(k_{xm}T_{xi})\cos(k_{yn}T_{yi})\cdot J_0(\sqrt{k_{xm}^2 + k_{yn}^2}\cdot a_i). \tag{17}$$

Similarly, using (10)–(13) to solve for K_2–K_4, we obtain

$$K_2 = K_3 = K_4 = 0 \tag{18}$$

because the integrands are combinations of orthogonal sinusoidal basis functions. We can solve α_2 in the same manner and by substituting the solutions of α_1 and α_2 into (8), the following expression is derived:

$$Z_{ij} = \frac{j\mu\omega d}{P_x P_y}\cdot\sum_{m=0}^{\infty}\sum_{n=0}^{\infty}\frac{C_m^2 C_n^2\cdot f_{\mathrm{cp}}}{k_{mn}^2 - k^2} \cdot\cos(k_{xm}T_{xi})\cos(k_{yn}T_{yi})\cos(k_{xm}T_{xj})\cos(k_{yn}T_{yj}) \tag{19}$$

Authorized licensed use limited to: Missouri University of Science and Technology. Downloaded on October 21,2024 at 21:00:28 UTC from IEEE Xplore. Restrictions apply.

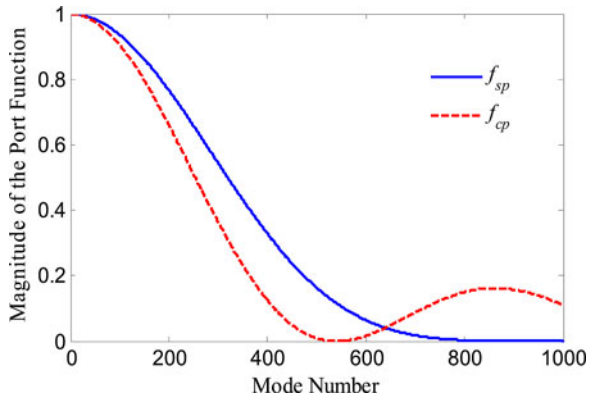

Fig. 3. Comparison of the port modulation function between circular port $f_{\rm cp}$ and square port $f_{\rm sp}$ of a square power-plane pair for mode number $m = n$. The ratio of the port radius to the plane width is 0.001.

where $k_{mn} = \sqrt{k_{xm}^2 + k_{yn}^2}$, $f_{\rm cp} = J_0(k_{mn}a_i) \cdot J_0(k_{mn}a_j)$.

Equation (19) can be considered as Green's function (6) modulated with $f_{\rm cp}$, resulting from the finite size of the circular port. In the formulation for square ports [4], this port modulation function is

$$f_{\rm sp} = \sin c\left(\frac{k_{xm}W_i}{2}\right) \cdot \sin c\left(\frac{k_{yn}W_i}{2}\right) \cdot \sin c\left(\frac{k_{xm}W_j}{2}\right) \cdot \sin c\left(\frac{k_{yn}W_j}{2}\right)$$

where W_i and W_j are the widths of ports i and j, respectively, which usually corresponds to the equivalent circular port diameter. It can be seen that, instead of *sinc* functions, the circular port expression (19) contains Bessel functions.

To give a first impression of the difference between the two functions, we consider the input impedance of a square power-plane pair with a port in the center. Suppose that the port radius is 1/1000 of the plane width and the square-port width equals the circular port diameter ($W = 2a$). Fig. 3 plots the two port modulation functions when $m = n$ and $k_{xm} = k_{yn}$. It can be observed that both functions converge to 1 for small arguments. However, the square-port approximation overestimates the contribution of the first hundreds of modes and diminishes the higher order modes beyond that. Therefore, the square-port model is only accurate in the low frequency range, where the impedance values are mainly determined by lower order modes.

It should be noted that the Green's function (6) represents modes in a PMC bounded rectangular cavity, sandwiched by two solid planes. However, an impedance is defined by assuming that a current is impressed on one port and all other ports remain open. This means that Z_{pp} should be calculated in the presence of open circular ports, i.e., PMC holes in the solid plane, whose Green's function is in general not known. The effect of these PMC holes should be included for an exact calculation of Z_{pp}. The impedance calculated by (19) can be considered as Z_{pp} in parallel connection to many small circular plane pairs, whose impedances can be found in [4]. The contribution of these small plane pairs can be excluded using the desegmentation technique [28].

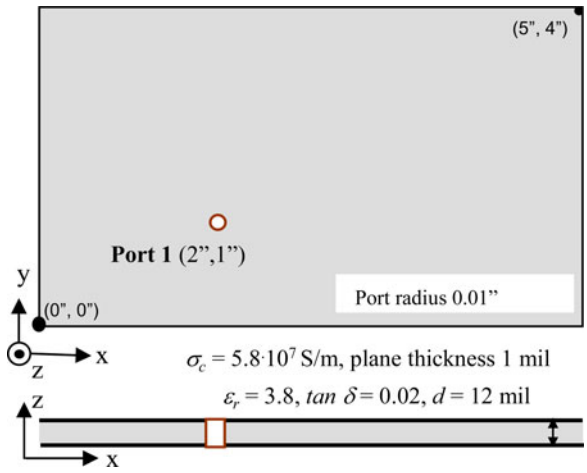

Fig. 4. Rectangular plane pair example with a single port. Dimensions are given in inches (1 mil = 0.001 in $\approx 25.4 \times 10^{-6}$ m).

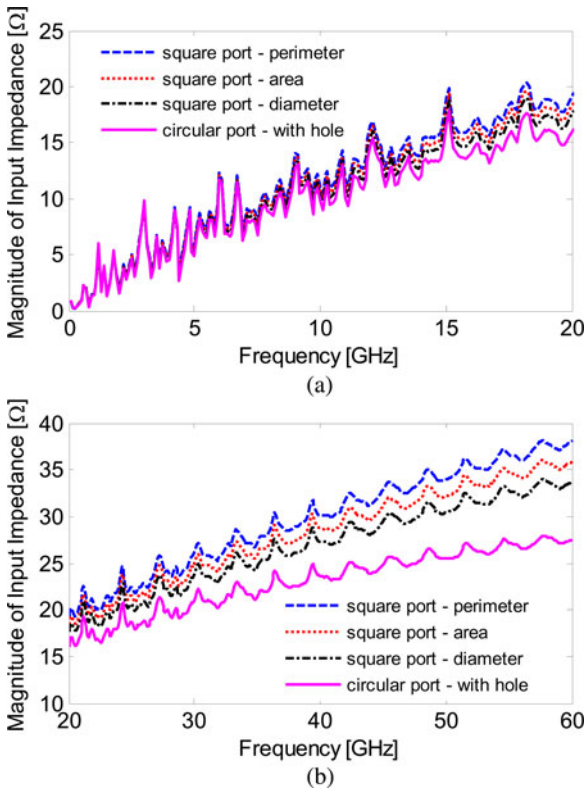

Fig. 5. Input impedance computed for the case in Fig. 4, obtained with the cavity model for circular port with the PMC hole and square port with equivalent perimeter, equivalent area, and equivalent diameter at frequencies (a) up to 20 GHz and (b) 20–60 GHz.

Fig. 4 shows a rectangular parallel-plate structure with a single port. We first evaluate the effect of port shape approximations on Z_{pp}. Fig. 5 plots the input impedance results calculated by the new approach for circular ports, compared to three approximated square-port cases, namely, equivalent perimeter ($W = \pi a/2$), equivalent area ($W = \sqrt{\pi} \cdot a$), and equivalent diameter ($W = 2a$). 1500∗1500 modes are used for all the calculations. It is observed that the impedance is almost not affected by the port shape at the frequencies below 10 GHz and mainly determined

Authorized licensed use limited to: Missouri University of Science and Technology. Downloaded on October 21,2024 at 21:00:28 UTC from IEEE Xplore. Restrictions apply.

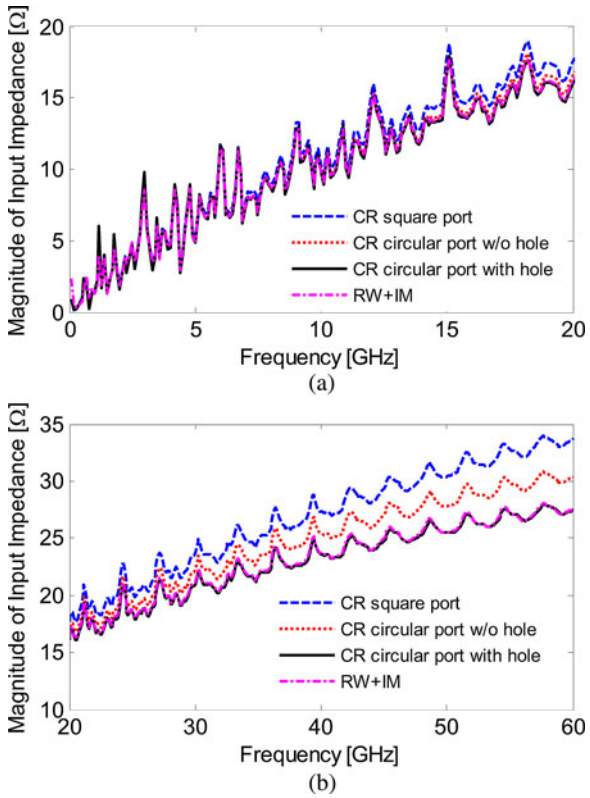

Fig. 6. Input impedance computed for the case in Fig. 4, obtained with the cavity model for square port, circular port with and without the PMC hole, as well as RW method plus image theory at frequencies (a) up to 20 GHz and (b) 20–60 GHz.

by the board resonances. However, at higher frequencies, where the board resonances are significantly damped by the loss, the square-port approximations overestimate the input impedance of the power planes, whereas the equivalent diameter approximation predicts the closest value to the circular port.

To demonstrate the effect of the PMC holes, the same configuration in Fig. 4 is computed with and without the PMC hole. The results are compared with the impedance obtained by the RW formula (4), combined with image theory, which is an efficient approach for the modeling of lossy rectangular power planes with circular ports [10]. The number of image layers is 10. As shown in Fig. 6, the result of circular port with the PMC hole overlaps with that calculated by the RW method, whereas higher impedance is predicted without extracting the small circular plates at frequencies higher than 20 GHz.

IV. CIM With Circular Ports

A. Infinite Planes

The CIM has been applied to calculate the power-plane impedances in [18]–[20]. In particular, circular ports have been modeled as discrete line segments circumscribing the port perimeters in [18]. However, accurate modeling of the ports in the high frequency range demands a large number of segments, which can dramatically increase the computation time. To avoid discretization of the ports, analytical expressions are derived

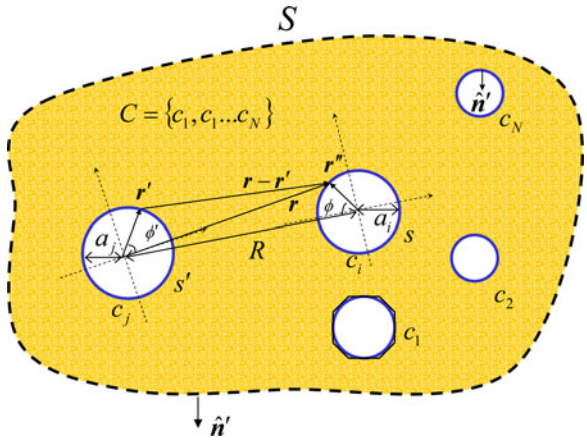

Fig. 7. Parameter definition for the CIM. Discretization of the circular port perimeter is illustrated for port c_1, which is only used when solving the ports numerically. S is the boundary of the power planes and R is the distance between the centers of the ports.

here. We start first by considering the boundary S, as shown in Fig. 7, at infinity. Since the larger the lossy power-plane pair is, the smaller the reflections from the boundary are, in the limit of infinite planes the reflection from the boundary is negligible. Hence, only the reflections from circular ports are necessary to be considered and an integral equation over the contours of the ports can be applied [4]

$$E_z(\boldsymbol{r}) = \frac{1}{2j}\cdot\oint_C \left[\frac{\partial H_0^{(2)}(k|\boldsymbol{r}-\boldsymbol{r}'|)}{\partial n}E_z(\boldsymbol{r}') - jk\eta\, H_0^{(2)}(k|\boldsymbol{r}-\boldsymbol{r}'|)\, i_n(\boldsymbol{r}')\right] ds' \tag{20}$$

where $\boldsymbol{r}$ and $\boldsymbol{r}'$ are the observation and source vectors on the contour C, respectively, which includes all the port perimeters $c_1, \ldots, c_N$, with N being the total number of ports. E_z and i_n are the tangential electric field and normal current density on the port contours, respectively. $\eta = \omega\mu_0/k$ denotes the complex wave impedance with ω being the angular frequency and μ_0 being the free space permeability. Under the assumption of isotropic excitation voltages and currents along the perimeters of source ports, (20) can be rewritten, according to voltage definition (2), as

$$V_i = -\sum_{j=1}^{N}\frac{V_j}{2j}\cdot\frac{1}{2\pi a_i}\cdot\underbrace{\oint_{c_i}\oint_{c_j}(\partial H_0^{(2)}(k|\boldsymbol{r}-\boldsymbol{r}'|)/\partial n)ds'ds}_{\beta_2} + \sum_{j=1}^{N}\frac{k\eta d}{4\pi a_j}\cdot I_j\cdot\frac{1}{2\pi a_i}\cdot\underbrace{\oint_{c_i}\oint_{c_j}H_0^{(2)}(k|\boldsymbol{r}-\boldsymbol{r}'|)ds'ds}_{\beta_1} \quad (i=1,\cdots,N) \tag{21}$$

where V_i and V_j are voltages on observation and source ports, respectively. $I_j = -2\pi a_j i_n(\boldsymbol{r}')$ is the total excitation current of the jth source port. Equation (21) can be expressed in matrix

Authorized licensed use limited to: Missouri University of Science and Technology. Downloaded on October 21,2024 at 21:00:28 UTC from IEEE Xplore. Restrictions apply.

form

$$\overline{\overline{U}}^{pp} \cdot \overline{V}^{p} = \overline{\overline{H}}^{pp} \cdot \overline{I}^{p} \tag{22}$$

where the identifier p denotes the circular ports, in contrast to line ports on the boundary of a finite plane, which will be introduced later. $\bar{V}^p$ and $\bar{I}^p$ are the voltage and current vectors, respectively, of size $(N \times 1)$. The integrals β_1 and β_2 will be obtained analytically in the following for the elements in matrices $\overline{\overline{H}}^{pp}$ and $\overline{\overline{U}}^{pp}$, respectively.

Using the addition theorem for Hankel functions [30] in the local cylindrical coordinate of the source port

$$H_0^{(2)}(k|\boldsymbol{r}-\boldsymbol{r}'|) = \sum_{n=-\infty}^{n=\infty} J_n\left(k\,|\boldsymbol{r}'|\right) \cdot H_n^{(2)}\left(k\,|\boldsymbol{r}|\right) \cdot e^{-jn\phi'} \tag{23}$$

the integral β_1 becomes

$$\beta_1 = a_i a_j \cdot \int_0^{2\pi} \left\{ \sum_{n=-\infty}^{n=\infty} \left[J_n(ka_j) H_n^{(2)}(k|\boldsymbol{r}|) \int_0^{2\pi} e^{-jn\phi'} d\phi' \right] \right\} d\phi \tag{24}$$

where ϕ' and ϕ are the angles in the local coordinate of source and observation ports, respectively. J_n and $H_n^{(2)}$ are the nth-order Bessel functions and Hankel functions of the second kind, respectively. The inner integral in (24) is only nonzero for $n = 0$. Hence, for $i = j$, $|\boldsymbol{r}| = a_j$ and the diagonal elements of $\overline{\overline{H}}^{pp}$ are derived as

$$H_{ij}^{pp} = \frac{k\eta d}{2} \cdot J_0(ka_j) H_0^{(2)}(ka_j) \quad (i = j). \tag{25}$$

For $i \neq j$, (24) is written as

$$\beta_1 = 2\pi a_i a_j \cdot J_0(ka_j) \cdot \int_0^{2\pi} H_0^{(2)}\left(k\,|\boldsymbol{r}|\right) d\phi. \tag{26}$$

The vector $\boldsymbol{r}$ can be expressed as $\boldsymbol{r} = (\boldsymbol{r} - \boldsymbol{r}'') - (-\boldsymbol{r}'')$, as shown in Fig. 7. Using again the addition theorem for Hankel function and $|-\boldsymbol{r}''| = a_i$, we obtain

$$\beta_1 = 2\pi a_i a_j \cdot J_0(ka_j) \cdot \sum_{n=-\infty}^{n=\infty} \left[J_n(ka_i) H_n^{(2)}(kR) \int_0^{2\pi} e^{-jn\phi} d\phi \right] \tag{27}$$

where $R = |\boldsymbol{r} - \boldsymbol{r}''|$, is the distance between the centers of source and observation ports, as shown in Fig. 7. The summation in (27) collapses to the term of $n = 0$. This leads to the solution of off-diagonal terms of $\overline{\overline{H}}^{pp}$

$$H_{ij}^{pp} = \frac{k\eta d}{2} \cdot J_0(ka_i) J_0(ka_j) H_0^{(2)}(kR) \quad (i \neq j). \tag{28}$$

For solving the matrix $\overline{\overline{U}}^{pp}$, the integral β_2 is expressed as

$$\beta_2 = -a_i a_j \cdot \int_0^{2\pi} \underbrace{\int_0^{2\pi} (\partial H_0^{(2)}(k|\boldsymbol{r}-\boldsymbol{r}'|)/\partial r') d\phi'}_{\beta_3} d\phi. \tag{29}$$

The integrand in (29) contains a first-order singularity for diagonal terms of $\overline{\overline{U}}^{pp}$, for which $\mathbf{r} = \mathbf{r}'$ is possible. We solve the off-diagonal terms first and evaluate the singularity for the diagonal terms later. Using again the addition theorem for Hankel functions and the recurrence relation for derivatives of Bessel functions, (29) is transformed to

$$\begin{aligned}\beta_2 &= -ka_i a_j \cdot \int_0^{2\pi} \int_0^{2\pi} \sum_{n=-\infty}^{n=\infty} \frac{J_{n-1}(ka_j) - J_{n+1}(ka_j)}{2} \\ &\quad \cdot H_n^{(2)}\left(k\,|\boldsymbol{r}|\right) \cdot e^{-jn\phi'} d\phi' d\phi \\ &= 2\pi k a_i a_j \cdot J_1(ka_j) \cdot \int_0^{2\pi} H_0^{(2)}\left(k\,|\boldsymbol{r}|\right) \cdot d\phi. \end{aligned} \tag{30}$$

The integral in (30) can be solved in a similar way as in (26) and we obtain the off-diagonal terms of $\overline{\overline{U}}^{pp}$

$$U_{ij}^{pp} = \frac{k\pi\, a_j}{j} \cdot J_0(ka_i) J_1(ka_j) H_0^{(2)}(kR) \quad (i \neq j). \tag{31}$$

For evaluation of the singularity for the diagonal terms, we rewrite the inner integral of (29) as

$$\begin{aligned}\beta_3 &= \lim_{\varepsilon \to 0} \left[\int_{\varepsilon}^{2\pi-\varepsilon} \frac{\partial H_0^{(2)}(k|\boldsymbol{r}-\boldsymbol{r}'|)}{\partial r'} d\phi' \right. \\ &\qquad \left. + \int_{-\varepsilon}^{\varepsilon} \frac{\partial H_0^{(2)}(k|\boldsymbol{r}-\boldsymbol{r}'|)}{\partial r'} d\phi' \right] \\ &= -2\pi k J_1(ka_j) \cdot H_0^{(2)}(ka_j) \\ &\quad + \lim_{\varepsilon \to 0} \underbrace{\int_{-\varepsilon}^{\varepsilon} k \cdot H_1^{(2)}(k|\boldsymbol{r}-\boldsymbol{r}'|) \cdot (|\boldsymbol{r}| \cos\phi' - |\boldsymbol{r}'|/|\boldsymbol{r}-\boldsymbol{r}'|) d\phi'}_{\beta_4}. \end{aligned} \tag{32}$$

To solve β_4, let us select an observation point just outside the source port, so that the small argument approximation for Hankel function, $H_1^{(2)}(z) = -2j/\pi z$, can be used. This leads to a simplification of β_4 as follows:

$$\begin{aligned}\beta_4 &= -\frac{2j}{\pi} \int_{-\varepsilon}^{\varepsilon} \frac{|\boldsymbol{r}| \cos\phi' - |\boldsymbol{r}'|}{|\boldsymbol{r} - \boldsymbol{r}'|^2} d\phi' \\ &= -\frac{4j}{\pi} \cdot \int_0^{\varepsilon} \frac{|\boldsymbol{r}| \cdot \cos\phi' - a_j}{|\boldsymbol{r}|^2 + a_j^2 - 2\,|\boldsymbol{r}| \cdot a_j \cos\phi'} d\phi'. \end{aligned} \tag{33}$$

With the help of an integral table [31], β_4 can be solved as

$$\beta_4 = -\frac{4j}{\pi} \cdot \left[-\frac{1}{2a_j}\varepsilon + \frac{1}{a_j} \cdot \arctan\left(\frac{|\boldsymbol{r}| + a_j}{|\boldsymbol{r}| - a_j} \cdot \tan\frac{\varepsilon}{2} \right) \right]. \tag{34}$$

Next, let the observation point approach the source port

$$\lim_{|\boldsymbol{r}| \to a_j^+} \beta_4 = \frac{2j}{\pi a_j} \cdot [\varepsilon - \pi]. \tag{35}$$

Substituting (35) into (32) leads to

$$\beta_3 = -2\pi k J_1(ka_j) \cdot H_0^{(2)}(ka_j) - \frac{2j}{a_j}. \tag{36}$$

Authorized licensed use limited to: Missouri University of Science and Technology. Downloaded on October 21,2024 at 21:00:28 UTC from IEEE Xplore. Restrictions apply.

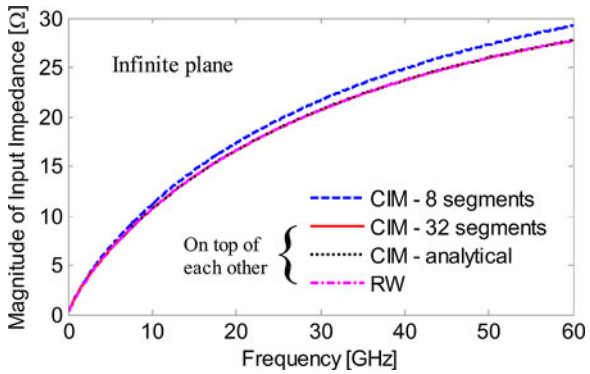

Fig. 8. Input impedance of a 10-mil radius port on an infinite plane pair, obtained with the CIM by discretizing the port perimeter with eight and 32 segments, the analytical solutions in (40), as well as the RW method. The material constants and dielectric height are defined as in Fig. 4. The simulation times for CIM-analytical and CIM-32 segments are 10 μs and 1.9 ms per frequency point, respectively.

Inserting (36) into (29), we obtain

$$\beta_2 = 2\pi a_i \cdot 2\pi a_j \cdot k \left[J_1(ka_j) \cdot H_0^{(2)}(ka_j) + \frac{j}{\pi k a_j} \right]. \quad (37)$$

Applying the Wronskian of Bessel functions [30]

$$J_1(z) \cdot H_0^{(2)}(z) = J_0(z) \cdot H_1^{(2)}(z) - \frac{2j}{\pi z} \quad (38)$$

and substituting (37), we obtain the diagonal terms of $\overline{\overline{U}}^{pp}$

$$U_{ij}^{pp} = \frac{k\pi a_j}{j} \cdot J_0(ka_j) H_1^{(2)}(ka_j) \quad (i = j). \quad (39)$$

Equations (25), (28), (31), and (39) constitute analytical expressions of all matrix elements in (22). The parallel-plate impedance of an infinite plane pair can then be calculated by

$$\overline{\overline{Z}}^{pp} = \overline{\overline{U}}^{pp^{-1}} \cdot \overline{\overline{H}}^{pp}. \quad (40)$$

Fig. 8 shows the input impedance of a circular port with 10-mil radius on an infinite plane pair, calculated using (40). The result is compared to the one obtained by discretizing the port into segments, as shown in Fig. 7 for the contour c_1, and taking average of voltages on the segments of the port assuming constant current excitation, as defined in (3). The material constants and dielectric height are the same as in Fig. 4. It can be observed that the impedance value predicted by modeling the port using eight segments is higher than that calculated by (40), whereas it converges to the result from (40), when the port is finer discretized into 32 segments, as shown in Fig. 8. The simulation time for the CIM with analytical solutions is 10 μs per frequency point, which is more than 100 times faster than the one by port discretized with 32 segments.

Note that in the low frequency range, where $ka \ll 1$, small argument approximations for Bessel functions can be used and the off-diagonal terms in $\overline{\overline{U}}^{pp}$ vanish. Equation (40) is reduced to (4), the RW equation for infinite planes. Therefore, the RW method is a low frequency approximation of our approach.

As stated in the last section, accurate computation of Z_{pp} should be done in the presence of PMC holes, i.e., with other ports open. The RW method does not take into account the scattering from the PMC holes, whose effect has been considered in (40) by the off-diagonal terms of $\overline{\overline{U}}^{pp}$. However, for input impedance calculation of a single port, the two methods are identical, as shown in Fig. 8.

B. Finite Boundary

Modeling of finite power planes using CIM has been described in [18], where the finite plane boundary contour S, as shown in Fig. 7, is discretized into M line segments with their widths much smaller than the wavelength. The segments can be considered as line ports, on which the voltages and currents are assumed to be constant. We combine these linear ports with the circular ports to form a new equation system as

$$\begin{bmatrix} \overline{\overline{U}}^{qq} & \overline{\overline{U}}^{qp} \\ \overline{\overline{U}}^{pq} & \overline{\overline{U}}^{pp} \end{bmatrix} \cdot \begin{bmatrix} \overline{V}^{q} \\ \overline{V}^{p} \end{bmatrix} = \begin{bmatrix} \overline{\overline{H}}^{qq} & \overline{\overline{H}}^{qp} \\ \overline{\overline{H}}^{pq} & \overline{\overline{H}}^{pp} \end{bmatrix} \cdot \begin{bmatrix} \overline{I}^{q} \\ \overline{I}^{p} \end{bmatrix} \quad (41)$$

where the index q denotes the line ports on the plane contour S with $\overline{V}^q$ and $\overline{I}^q$ being the voltage and current vectors on them, respectively. The following impedance matrix can be obtained:

$$\begin{bmatrix} \overline{\overline{Z}}^{qq} & \overline{\overline{Z}}^{qp} \\ \overline{\overline{Z}}^{pq} & \overline{\overline{Z}}^{pp} \end{bmatrix} = \begin{bmatrix} \overline{\overline{U}}^{qq} & \overline{\overline{U}}^{qp} \\ \overline{\overline{U}}^{pq} & \overline{\overline{U}}^{pp} \end{bmatrix}^{-1} \cdot \begin{bmatrix} \overline{\overline{H}}^{qq} & \overline{\overline{H}}^{qp} \\ \overline{\overline{H}}^{pq} & \overline{\overline{H}}^{pp} \end{bmatrix}. \quad (42)$$

Under the assumption of a PMC boundary condition, i.e., $\overline{I}^q = 0$, $\overline{\overline{Z}}^{pp}$ represents then the parallel-plate impedance of the finite plane pair. The matrix entries in (42) are calculated as

$$U_{ij}^{qq} = \delta_{ij} - \frac{k}{2j} \int_{W_j} \hat{\boldsymbol{R}} \cdot \hat{\boldsymbol{n}}' H_1^{(2)}(k|\boldsymbol{r}_i - \boldsymbol{r}_j|) ds' \quad (42a)$$

$$H_{ij}^{qq} = \begin{cases} \dfrac{k\eta d}{2} \dfrac{1}{W_j} \displaystyle\int_{W_j} H_0^{(2)}(k|\boldsymbol{r}_i - \boldsymbol{r}_j|) ds' & (i \neq j) \\ \dfrac{k\eta d}{2} \left[1 - \dfrac{2j}{\pi} \left(\ln\left(\dfrac{kW_i}{4} \right) - 1 + \gamma \right) \right] & (i = j) \end{cases} \quad (42b)$$

$$U_{ij}^{qp} = \frac{k\pi a_j}{j} \cdot J_1(ka_j) H_0^{(2)}(kR) \quad (42c)$$

$$H_{ij}^{qp} = \frac{k\eta d}{2} \cdot J_0(ka_j) H_0^{(2)}(kR) \quad (42d)$$

$$U_{ij}^{pq} = -\frac{k}{2j} \cdot J_0(ka_i) \cdot \int_{W_j} \hat{\boldsymbol{R}} \cdot \hat{\boldsymbol{n}}' H_1^{(2)}(k|\boldsymbol{r}_i - \boldsymbol{r}_j|) ds' \quad (42e)$$

$$H_{ij}^{pq} = \frac{k\eta d}{2} \cdot J_0(ka_i) \cdot \frac{1}{W_j} \int_{W_j} H_0^{(2)}(k|\boldsymbol{r}_i - \boldsymbol{r}_j|) ds' \quad (42f)$$

where δ_{ij} is the Kronecker's delta and $\gamma = 0.5772$ is the Euler's constant. $\boldsymbol{r}_j$ is the vector of source points on the boundary line port whose width is represented by W_j. $\boldsymbol{r}_i$ is the observation vector at the center of the linear or circular port. $\hat{\boldsymbol{n}}'$ denotes the unit normal vector on boundary S. $\hat{\boldsymbol{R}}$ represents the normalized vector of $\boldsymbol{r}_i - \boldsymbol{r}_j$. $\overline{\overline{U}}^{pp}$ and $\overline{\overline{H}}^{pp}$ are obtained with (25), (28), (31), and (39). In contrast to the original formulation of the CIM, which contains only (42a) and (42b) [4], [18]–[20], (42c)–(42f)

Authorized licensed use limited to: Missouri University of Science and Technology. Downloaded on October 21,2024 at 21:00:28 UTC from IEEE Xplore. Restrictions apply.

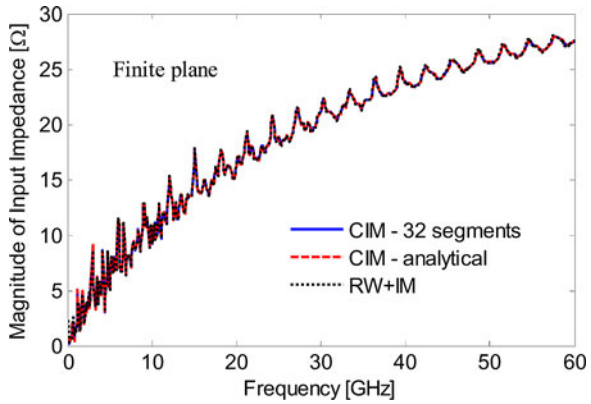

Fig. 9. Input impedance computed for the case in Fig. 4, obtained with the CIM by discretizing the port perimeter, CIM with analytical circular port solution, and RW method plus image theory. The simulation times for CIM-analytical and CIM-32 segments are 13.8 and 14.3 s per frequency point, respectively.

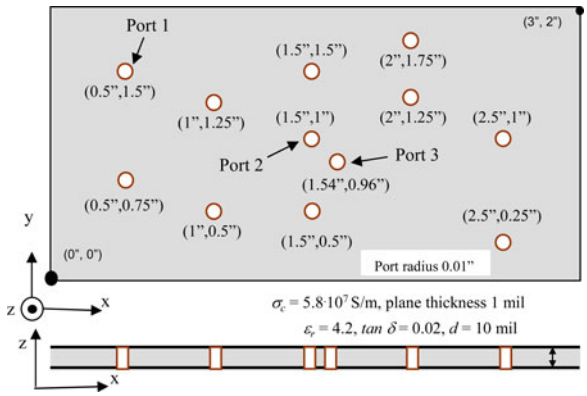

Fig. 10. Rectangular plane pair example with 12 ports. Dimensions are given in inches (1 mil = 0.001 in $\approx 25.4 \times 10^{-6}$ m).

are additionally included as a result of the analytical solutions with regard to circular ports derived in this paper.

Note that the method described previously is suitable for lossy structures, i.e., k is complex, which is the case for most of the practical applications. For lossless structures, the method can be imprecise especially near resonance frequencies due to bad conditioning of the matrix.

Fig. 9 plots the simulated input impedance for the case shown in Fig. 4 using the approach described previously in (42), compared to the results from the original CIM by discretizing the port perimeter, and the RW method combined with image theory. The three methods yield identical results. The simulation time for the CIM with analytical solutions is 13.8 s per frequency point, a slight improvement in contrast to 14.3 s per frequency point with 32 segments since the number of unknowns associated with boundary ports dominates in this case.

V. Further Application and Discussion

In accordance with the circular port assumption (1), (2), and (3), three methods, the RW algorithm, the CR model, and the CIM, have been discussed in this paper. We have shown the equivalence among them when modeling a single port. Here, we extend the comparison to a 12-port example, as shown in Fig. 10, whereas the input impedance of port 1 and the transfer impedance between ports 2 and 3 will be demonstrated.

Considering first the case of infinite planes, i.e., without boundaries, which can only be modeled by RW and CIM methods, the input impedance Z_{11} and transfer impedance Z_{23} are plotted in Figs. 11 and 12, respectively. As discussed before, the RW method is a low frequency approximation of the CIM derived previously. The two curves for Z_{11} are almost not distinguishable from each other due to the fact that the distances from port 1 to other ports are relatively far and the scattered field from other ports has negligible influence on the input impedance of port 1. However, it can been seen for Z_{23} that the two curves start to deviate at about 15 GHz, since the two ports are close to each other and the scattered field from open ports takes effect.

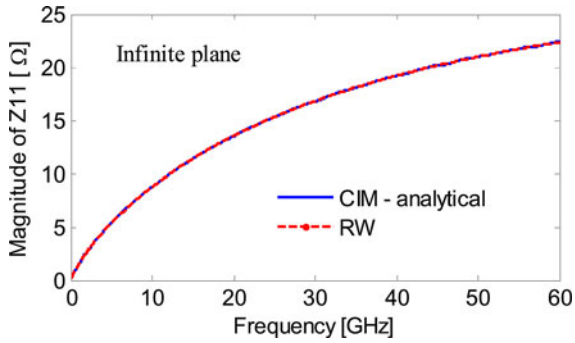

Fig. 11. Input impedance of port 1, as shown in Fig. 10, without considering the plane boundary, obtained by the CIM with analytical solutions and the RW method.

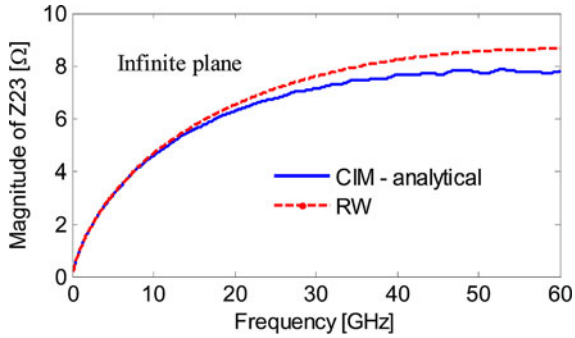

Fig. 12. Transfer impedance between ports 2 and 3, as shown in Fig. 10, without considering the plane boundary, obtained by the CIM with analytical solutions and the RW method.

Similar behavior can be observed for finite planes, as shown in Figs. 13 and 14 for Z_{11} and Z_{23}, respectively. All three methods predict almost the same input impedance at port 1, whereas for the transfer impedance Z_{23}, the CR model predicts identical results as the CIM, since they share the same impedance definition, but the RW method plus images overestimates Z_{23} for frequencies above 20 GHz due to the fact that reflections from open ports are not taken into account. At very low frequencies (up to 2 GHz), the results from RW method plus image theory also differs slightly from the other two due to insufficient number of image layers. The agreement can be improved by adding more image layers.

Authorized licensed use limited to: Missouri University of Science and Technology. Downloaded on October 21,2024 at 21:00:28 UTC from IEEE Xplore. Restrictions apply.

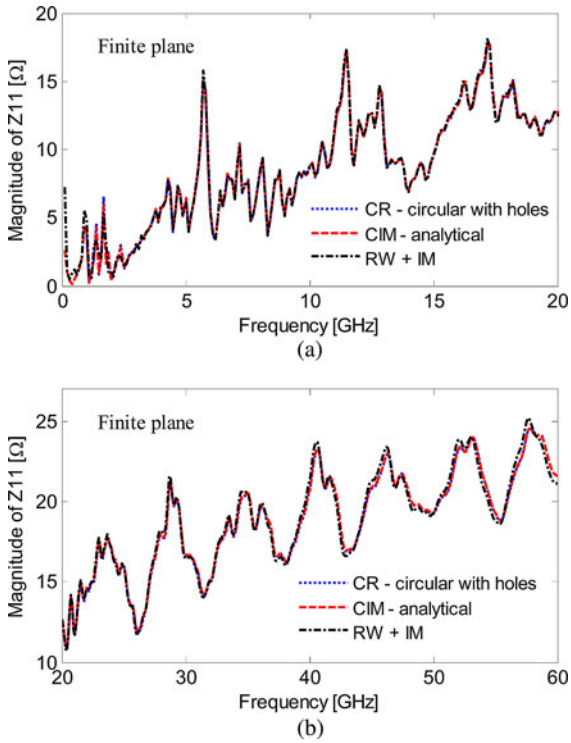

Fig. 13. Input impedance of port 1, computed for the 12-port case of a finite plane pair, as shown in Fig. 10, obtained with the CR circular model with PMC holes, CIM with analytical solutions, and RW method plus image theory at frequencies (a) up to 20 GHz and (b) 20–60 GHz. 1500∗1500 modes are used in the CR model.

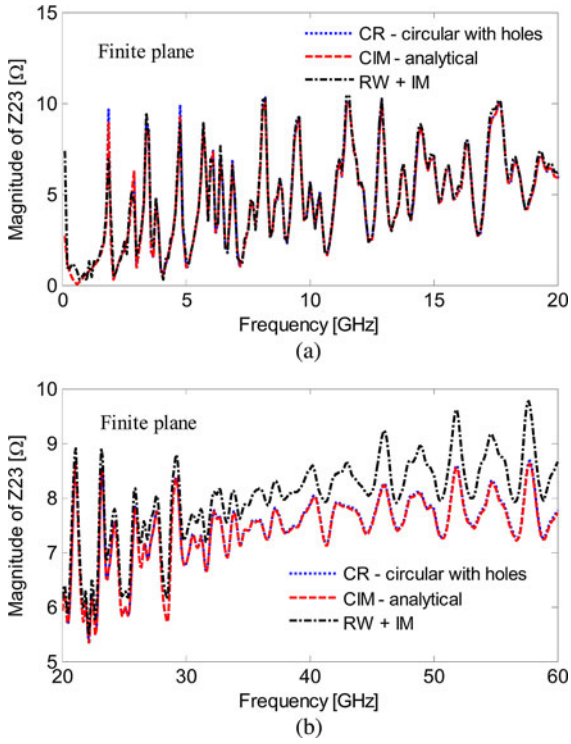

Fig. 14. Transfer impedance between ports 2 and 3, computed for the 12-port case of a finite plane pair, as shown in Fig. 10, obtained with the CR circular model with PMC holes, CIM with analytical solutions, and RW method plus image theory at frequencies (a) up to 20 GHz and (b) 20–60 GHz. 1500∗1500 modes are used in the CR model.

TABLE I
CPU TIME FOR THE FINITE PLANE CASE IN FIG. 10 USING CIM WITH DIFFERENT NUMBER OF CIRCULAR PORTS

Number of Circular Ports	Numerical 8 segments	Numerical 16 segments	Numerical 32 segments	Analytical
1	2.5	2.5	2.7	2.4
6	2.9	3.5	4.9	2.5
12	3.5	4.9	8.9	2.5
25	5.0	5.3	24.7	2.6

Unit in second per frequency point.
Simulation was run on a 64-bit PC with 2.8 GHz CPU.

VI. CONCLUSION

The CR model and the CIM have been extended based on an isotropic excitation field assumption at circular ports. Analytical expressions have been derived for more accurate calculation of the parallel-plate impedances. In comparison to the RW method, the two extended methods also take into account the scattering effect from open ports. The methods discussed here can be easily incorporated into the via models, in [23]–[25], for fast and accurate analysis of multilayer structures.

Furthermore, the efficiency of CIM has also been improved by using the analytical solutions instead of discretizing the port perimeter. This is especially true when the number of circular ports dominates. As shown in Table I, the speed up is increased from a factor of 1.1 for the 1-port case to a factor of 10 for the 25-port case, when comparing the CPU time using analytical solution to the numerical one with 32 segments.

It should be stated that the assumptions in Section II do not reflect a full-wave field distribution on the port, since the line integrals rule out any anisotropic modes on the port. The inclusion of their effect will be the future work of the authors.

ACKNOWLEDGMENT

The authors would like to thank Dr. J. Fan and Dr. Y. J. Zhang from the Missouri University of Science and Technology, Rolla, and Dr. B. Archambeault, Dr. X. Gu, Dr. Y. Kwark, and Dr. M. Ritter from IBM for constructive discussions and communications.

REFERENCES

[1] J. Park, H. Kim, Y. Jeong, J. Kim, J. S. Pak, D. G. Kam, and J. Kim, "Modeling and measurement of simultaneous switching noise coupling through signal via transition," *IEEE Trans. Adv. Packag.*, vol. 29, no. 3, pp. 548–559, Aug. 2006.

[2] W. Cui, J. Fan, Y. Ren, H. Shi, J. L. Drewniak, and R. E. DuBroff, "DC power-bus noise isolation with power-plane segmentation," *IEEE Trans. Electromagn. Compat.*, vol. 45, no. 2, pp. 436–443, May 2003.

[3] C. Schuster and W. Fichtner, "Parasitic modes on printed circuit boards and their effects on EMC and signal integrity," *IEEE Trans. Electromagn. Compat.*, vol. 43, no. 4, pp. 416–425, Nov. 2000.

[4] T. Okoshi, *Planar Circuits for Microwaves and Lightwaves*. Berlin, Germany: Springer-Verlag, 1985.

[5] G. T. Lei, R. W. Techentin, P. R. Hayes, D. J. Schwab, and B. K. Gilbert, "Wave model solution to the ground/power plane noise problem," *IEEE Trans. Instrum. Meas.*, vol. 44, no. 2, pp. 300–303, Apr. 1995.

[6] G. T. Lei, R. W. Techentin, and B. K. Gilbert, "High-frequency characterization of power/ground-plane structures," *IEEE Trans. Microw. Theory Tech.*, vol. 47, no. 5, pp. 562–569, May 1999.

[7] C. Wang, J. Mao, G. Selli, S. Luan, L. Zhang, J. Fan, D. J. Pommerenke, R. E. DuBroff, and J. L. Drewniak, "An efficient approach for power delivery network design with closed-form expressions for parasitic interconnect

Authorized licensed use limited to: Missouri University of Science and Technology. Downloaded on October 21,2024 at 21:00:28 UTC from IEEE Xplore. Restrictions apply.

inductances," *IEEE Trans. Adv. Packag.*, vol. 29, no. 2, pp. 320–334, May 2006.
[8] N. Na, J. Choi, S. Chun, M. Swaminathan, and J. Srinivasan, "Modeling and transient simulations of planes in electronic packages," *IEEE Trans. Adv. Packag.*, vol. 23, no. 3, pp. 340–352, Aug. 2000.
[9] Z. L. Wang, O. Wada, Y. Toyota, and R. Koga, "Convergence acceleration and accuracy improvement in power bus impedance calculation with a fast algorithm using cavity modes," *IEEE Trans. Electromagn. Compat.*, vol. 47, no. 1, pp. 2–8, Feb. 2005.
[10] R. Rimolo-Donadio, H.-D. Brüns, and C. Schuster, "Hybrid approach for efficient calculation of the parallel-plate impedance of lossy power/ground planes," *Microw. Opt. Technol. Lett.*, vol. 51, no. 9, pp. 2051–2056, Sep. 2009.
[11] J. C. Parker, "Via coupling within parallel rectangular planes," *IEEE Trans. Electromagn. Compat.*, vol. 39, no. 1, pp. 17–25, Feb. 1997.
[12] R. Ito, R. W. Jackson, and T. Hongsmatip, "Modeling of interconnections and isolation within a multilayered ball grid array package," *IEEE Trans. Microw. Theory Tech.*, vol. 47, no. 9, pp. 1819–1825, Sep. 1999.
[13] A. R. Chada, Y. Zhang, G. Feng, J. L. Drewniak, and J. Fan, "Impedance of an infinitely large parallel-plate pair and its applications in engineering modelling," in *Proc. IEEE Int. Symp. Electromagn. Compat.*, Austin, TX, Aug. 2009, pp. 78–82.
[14] M. Xu and T. H. Hubing, "The development of a closed-form expression for the input impedance of power-return plane structures," *IEEE Trans. Electromagn. Compat.*, vol. 45, no. 3, pp. 478–485, Aug. 2003.
[15] J. Trinkle and A. Cantoni, "Impedance expressions for unloaded and loaded power ground planes," *IEEE Trans. Electromagn. Compat.*, vol. 50, no. 2, pp. 390–398, May 2008.
[16] H. Chen, Q. Li, L. Tsang, C. C. Huang, and V. Jandhyala, "Analysis of a large number of vias and differential signalling in multilayered structures," *IEEE Trans. Microw. Theory Tech.*, vol. 51, no. 3, pp. 818–829, Mar. 2003.
[17] Z. Z. Oo, E. X. Liu, E. P. Li, X. Wei, Y. Zhang, M. Tan, L. W. J. Li, and R. Vahldieck, "A semi-analytical approach for system-level electrical modeling of electronic packages with large number of vias," *IEEE Trans. Adv. Packag.*, vol. 31, no. 2, pp. 267–274, May 2008.
[18] M. Strumpf and M. Leone, "Efficient 2-D integral equation approach for the analysis of power bus structures with arbitrary shape," *IEEE Trans. Electromagn. Compat.*, vol. 51, no. 1, pp. 38–45, Feb. 2009.
[19] X. Wei, E. Li, E. Liu, and X. Cui, "Efficient modeling of rerouted return currents in multilayered power-ground planes by using integral equation," *IEEE Trans. Electromagn. Compat.*, vol. 50, no. 3, pp. 740–743, Aug. 2008.
[20] X. Duan, R. Rimolo-Donadio, H. Brüns, B. Archambeault, and C. Schuster, "Special session on power integrity techniques: Contour integral method for rapid computation of power/ground plane impedance," presented at the IEC DesignCon Conf., Santa Clara, CA, Feb. 2010.
[21] Y. Zhang, G. Feng, and J. Fan, "A novel impedance definition of a parallel-plate pair for an intrinsic via circuit model," *IEEE Trans. Microw. Theory Tech.*, vol. 58, no. 12, pp. 3780–3789, Aug. 2010.
[22] D. G. Kam, M. B. Ritter, T. J. Beukema, J. F. Bulzacchelli, P. K. Pepeljugoski, Y. H. Kwark, S. Lei, X. Gu, C. W. Baks, R. A. John, G. Hougham, C. Schuster, R. Rimolo-Donadio, and B. Wu, "Is 25 Gb/s on-board signalling viable?," *IEEE Trans. Adv. Packag.*, vol. 32, no. 2, pp. 328–344, May 2009.
[23] X. Gu, R. Rimolo-Donadio, Z. Yu, F. D. Paulis, Y. H. Kwark, M. Cocchini, M. B. Ritter, B. Archambeault, A. Ruehli, J. Fan, and C. Schuster, "Fast-physics-based via and trace models for signal and power integrity co-analysis," presented at the IEC DesignCon Conf., Santa Clara, CA, Feb. 2010.
[24] R. Rimolo-Donadio, X. Gu, Y. H. Kwark, M. B. Ritter, B. Archambeault, F. D. Paulis, Y. Zhang, J. Fan, H.-D. Brüns, and C. Schuster, "Physics-based via and trace models for efficient link simulation on multilayer structure up to 40 GHz," *IEEE Trans. Microw. Theory Tech.*, vol. 57, no. 8, pp. 2072–2083, Aug. 2009.
[25] Y. Zhang and J. Fan, "An intrinsic circuit model for multiple vias in an irregular plate pair through rigorous electromagnetic analysis," *IEEE Trans. Microw. Theory Tech.*, vol. 58, no. 8, pp. 2251–2265, Aug. 2010.
[26] X. Duan, R. Rimolo-Donadio, H. Brüns, and C. Schuster, "A combined method for fast analysis of signal propagation, ground noise, and radiated emission of multilayer printed circuit boards," *IEEE Trans. Electromagn. Compat.*, vol. 52, no. 2, pp. 487–495, May 2010.
[27] J. Kim, Y. Jeong, J. Kim, J. Lee, C. Ryu, J. Shim, M. Shin, and J. Kim, "Modeling and measurement of interlevel electromagnetic coupling and fringing effect in a hierarchical power distribution network using segmentation method with resonant cavity model," *IEEE Trans. Adv. Packag.*, vol. 31, no. 3, pp. 544–557, Aug. 2008.
[28] K. C. Gupta and M. D. Abouzahra, Eds., *Analysis and Design of Planar Microwave Components*. Piscataway, NJ: IEEE Press, 1994, ch. 3.
[29] M. Abramowitz and I. A. Stegun, *Handbook of Mathematical Functions*. New York: Dover, 1965.
[30] C. A. Balanis, *Advanced Engineering Electromagnetics*. New York: Wiley, 1989, ch. 11.
[31] I. S. Gradshteyn and I. M. Ryzhik, *Table of Integrals, Series, and Products*. New York: Academic, 1980, p. 148.

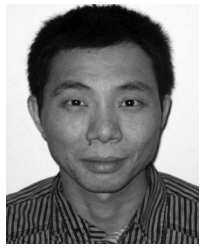

Xiaomin Duan (S'08) received the B.S. degree in electrical engineering from Zhejiang University, Hangzhou, China, in 2002. He received the M.S. degree in microelectronics and microsystems from the Technical University Hamburg-Harburg, Hamburg, Germany, in 2007, where he is currently working toward the Ph.D. degree from the Institute of Electromagnetic Theory.

His research interests include application and extension of the method of moments to the electrical analysis of print circuit boards in high-speed digital systems.

Mr. Duan received the IEEE Electromagnetic Compatibility Best Student Symposium Paper Award in 2009 and an IBM Ph.D. Fellowship Award in 2010.

Renato Rimolo-Donadio (S'08–M'11) received the B.S. and Lic. degrees in electrical engineering from the Technical University of Costa Rica, Cartago, Costa Rica, in 1999 and 2004, respectively. He received the M.S. degree in microelectronics and microsystems (with distinction) and the Ph.D. degree in electrical engineering (*summa cum laude*) both from the Technical University of Hamburg-Harburg (TUHH), Hamburg, Germany, in 2006 and 2010, respectively.

Since January 2011, he has been a Postdoctoral Research Assistant with the Institute of Electromagnetic Theory, TUHH. His research interests include system-level modeling and optimization of interconnects, and analysis of signal and power integrity problems at printed circuit board and package levels.

Heinz-Dietrich Brüns was born in Bremerhaven, Germany, in 1953. He received the Diploma in electrical engineering from the Technische Universität Braunschweig, Brunswick, Germany, and the Ph.D. degree from the Universität der Bundeswehr, Hamburg, Germany, in 1980 and 1985, respectively.

Since 1985, he has been with the Technical University of Hamburg-Harburg, Hamburg. His research interests include method of moments and numerical techniques in electromagnetics.

Christian Schuster (S'98–M'00–SM'05) received the Diploma degree in physics from the University of Konstanz, Konstanz, Germany, and the Ph.D. degree in electrical engineering from the Swiss Federal Institute of Technology, Zurich, Switzerland, in 1996 and 2000, respectively.

Since 2006, he has been a Full Professor and the Head of the Institute of Electromagnetic Theory, Technical University of Hamburg-Harburg (TUHH), Hamburg, Germany. Prior to that he was with the IBM T. J. Watson Research Center, Yorktown Heights, NY, where he was involved in high-speed optoelectronic package and backplane interconnect modeling and signal integrity design for new server generations. His research interests include signal and power integrity of digital systems, multiport measurement and calibration techniques, and development of electromagnetic simulation methods for communication electronics.

Dr. Schuster received the IEEE Transactions on Electromagnetic Compatibility (EMC) Best Paper Award in 2001, IEC DesignCon Paper Awards in 2005, 2006, and 2010, three IBM Research Division Awards between 2003 and 2005, IBM Faculty Awards in 2009 and 2010, and an Award for the best interactive presentation at DATE-Europe in 2009. He is a member of the German Physical Society and several technical program committees of international conferences on signal and power integrity and electromagnetic compatibility.

Authorized licensed use limited to: Missouri University of Science and Technology. Downloaded on October 21,2024 at 21:00:28 UTC from IEEE Xplore. Restrictions apply.